Neuronal Population Dynamics with Post Inhibitory Rebound: A Reduction to Piecewise Linear Discontinuous Circle Maps

S Coombes & S H Doole
Department of Engineering Mathematics,
Bristol University,
University Walk,
Bristol, BS8 1TR, UK
s.coombes@bristol.ac.uk stuart.doole@bristol.ac.uk

May 20, 1996

Abstract

Post inhibitory rebound is a nonlinear phenomenon present in a variety of nerve cells. It is an important mechanism underlying central pattern generation for heartbeat, swimming and other motor patterns in many neuronal systems. In this paper we propose an extension of the binary threshold neuron model to incorporate the effects of post inhibitory rebound. For a single neuron, the dynamics can be described by a piecewise linear circle map with two discontinuities. Both frequency-locking and chaos can occur. The Liapunov exponent of the map is evaluated and used to define transitions between these two distinct types of asymptotic behaviour. Hysteresis between periodic orbits is also observed.

A small network of these model neurons, with reciprocal inhibition, is shown to exhibit *self-sustained* anti-phase oscillations, making post inhibitory rebound a plausible mechanism for central pattern generation in neuronal systems. Unlike coupled oscillator theories, network oscillations emerge naturally as a consequence of the biological description from which the neuronal dynamics is derived. The simplicity of the dynamical model allows for the possibility of large population studies in contrast to other classical models of single neuron dynamics that incorporate active processes.

KEYWORDS
Central pattern generation, Circle maps, Neuronal dynamics, Piecewise linear, Post inhibitory rebound, Reciprocal inhibition.

Acknowledgments
The authors thank Professor Paul Glendinning (Mathematics, QMW, London) and Professor Alan Roberts & Craig Green (School of Biological Sciences, Bristol) for helpful comments during the completion of this work.

1 Introduction

Recordings from nerve cells demonstrate that if the potential at the cell body or soma is increased above a certain threshold value, then a pulse-like signal can be initiated along the outgoing axon. Such action potentials are actively regenerated in a nonlinear fashion as they travel along the axon. Neither the strength nor the amplitude of the action potential is influenced by the original stimulus. Hence, nerve cells are often caricatured by all-or-nothing threshold devices. In addition to the action potential, one other important nonlinear phenomenon in a variety of nerve cells is *post inhibitory rebound* (PIR). This is an active process in which the excitability of the neuron is enhanced temporarily following a period of voltage depression (*hyper-polarisation*).

Post inhibitory rebound has been shown experimentally to play an important role in central pattern generating networks that produce rhythmic output (Arbas & Calabrese 1987*b*, Arshavsky, Orlovsky, Panchin, Roberts & Soffe 1993, Roberts 1990, Satterlie 1985). The theoretical importance of post inhibitory rebound for central pattern generation in networks of non-oscillatory neurons was first recognised by Perkel and Mulloney (1974) and has recently been reviewed by Calabrese (1995). (A broad review of central pattern generation in neuronal networks can be found in Getting (1988), Mulloney & Perkel (1988).) The mechanism of post inhibitory rebound may also have a role within the context of thalamocortical oscillations, driven by reticular thalamic neurons, which arise from interactions between solely inhibitory neurons (Golomb, Wang & Rinzel 1994, Steriade, Jones & Linas 1990). In certain nerve cells, such as those of the medicinal leech, the ionic mechanism for post inhibitory rebound has been uncovered (Angstadt & Calabrese 1989, Arbas & Calabrese 1987*a*). Numerical studies of Hodgkin-Huxley kinetics with hyper-polarisation-activated inward currents have also been shown to exhibit post inhibitory rebound (Kopell & LeMasson 1994).

Roberts and Tunstall (1990) modelled locomotor rhythm generation in the spinal cord of the *Xenopus* tadpole embryo using computer simulations of a small network of Hodgkin-Huxley neurons with reciprocal inhibition and self excitation. The network supports self-sustained firing and the output closely resembles the spinal cord motor pattern during swimming. Post inhibitory rebound is an emergent property of the non-linear membrane dynamics and is necessary for the production of the rhythmic firing patterns. Related results have been obtained in simpler networks (Mulloney, Perkel & Budelli 1981, Perkel & Mulloney 1974, Perkel, Mulloney & Budelli 1995). Using a neuron model that includes synaptic conductance changes and action potentials, they showed that a pair of neurons connected through reciprocally inhibitory synapses can exhibit a stable pattern of alternating bursts. Unfortunately, in an attempt to mimic post inhibitory rebound, their model introduces a state variable which has no biological interpretation. The same network with Moris-Lecar type dynamics has also been shown to exhibit oscillatory behaviour (Skinner, Kopell & Marder 1994, Skinner, Turrigiano & Marder 1993).

Dynamical equations such as Hodgkin-Huxley (1952), Fitzhugh-Nagumo (1961) and Moris-Lecar (1981) are used to model single neuron dynamics with active processes. However, they are difficult to analyse explicitly when modelling populations of neurons. Often, simpler single neuron studies can provide a more appropriate starting point for the discussion of network properties. Such a model of active membrane dynamics must incorporate features such as post inhibitory rebound. Within the field of artificial neural networks, it is common to consider networks of McCulloch-Pitts (1943) neurons. Here the presence of an action potential is sig-

nalled by the firing of a two-state threshold element. A more biologically inspired model of a neuron than that of McCullogh and Pitts has been presented by Bressloff and Taylor – for a review see (Bressloff & Taylor 1991). Their binary neuron is based upon a dynamical description of the membrane potentials in terms of 'leaky integrator' shunting equations. As in the McCulloch-Pitts neuron, firing is a nonlinear function of the current neuron activity. However, the current activation state of each neuron is now a function of the neurons previous output activity stretching back to the initial time (extended time summation). This model yields a discrete time framework for investigating coherent oscillatory behaviour in neuronal populations. However, post inhibitory rebound is not accommodated and nor is it an emergent property.

In this paper we model post inhibitory rebound at a level of description comparable with that of Bressloff and Taylor. Since the appearance of an action potential is modelled by the activation of a threshold element, we incorporate post inhibitory rebound in the same fashion, that is, with a threshold for *rebounding*. Importantly, and unlike previous descriptions of post inhibitory rebound, for example Mulloney (1981), all model parameters may be found from existing experimental data.

In Section 2 we consider a neuronal population dynamics based upon the leaky integrator model with shunting inhibition in which details of synaptic time delay and post inhibitory rebound are included. The explicit integration of these equations is performed for the case of pulse-like neuronal signals. The result is a set of difference equations describing network evolution. In Section 3, we reduce the dynamics for a single neuron to a piecewise linear circle map with two discontinuities. We study how the dynamics of this map vary with a bifurcation parameter which represents the size of the global input from a surrounding neuronal network. Both quasi-periodicity and chaos can occur: to define transitions between these two asymptotic behaviours, the Liapunov exponent of the map can be evaluated in terms of the corresponding rotation number. In particular, we observe transitions from quasi-periodicity to chaos and back again. For biologically realistic parameter values, the hysteretic transitions between certain periodic orbits illustrate the rich dynamic behaviour of our basic neuron.

In Section 4, we consider a network of 2 model neurons with reciprocal inhibitory synapses, incorporating post inhibitory rebound. The network supports self-sustained anti-phase oscillation in good qualitative agreement to related models of gastric rhythm generation for decapod crustaceans (Wang & Rinzel 1992). In contrast the same network without post inhibitory rebound cannot oscillate.

Finally, we discuss the extensions of this work to incorporate delays on different time scales together with the effect of local electrical synaptic coupling upon neuronal population dynamics with post inhibitory rebound. Amongst other advantages, these modifications allow for accurate quantitative agreement between the model and the neurobiological phenomena. Hence the proposed neuron model is a suitable basis for large population studies of neurons with the appropriate biological architecture.

2 Neuronal population dynamics with PIR

Single neuron equations that reproduce all the behaviour of a biological neuron can be used as the basic elements for a study of neuronal population dynamics. Previous analysis of a

discrete-time binary single-neuron model incorporating the effects of refractoriness demonstrates the possibility of periodic neuronal response characteristics (Aihara, Takabe & Toyada 1990). More recently Bressloff & Taylor (1991) have discussed such models with temporal features that capture the fact that cell membrane potential decay has a typical time course. Moreover, their model has the added advantage of being derived from biological principles with realistic descriptions of neuronal input in the form of synaptic shunting currents. Interestingly, this model allows for the possibility of a chaotic response. However, one feature of a single neuron that their model does not describe is that of post inhibitory rebound. With this in mind, we define the following model of N leaky integrators with post inhibitory rebound. Let $V_i(t)$ be the membrane potential of the i^{th} neuron at time t with respect to some resting potential. Then $V_i(t)$ satisfies the differential equation

$$C_i \frac{\mathrm{d}V_i(t)}{\mathrm{d}t} = -\frac{V_i(t)}{R_i} + \sum_{j=1}^{N} \Delta g_{ij}(t)[S_{ij} - V_i(t)] + \Delta g_i(t) S_i \,, \tag{1}$$

where C_i, R_i are the ith membrane capacitance and resistance respectively; and $\Delta g_{ij}(t)$, $i \neq j$, the synaptic conductance change at synapse $(i,\ j)$ with membrane reversal potential S_{ij}. Excitatory synapses have positive reversal potentials while inhibitory ones have negative reversal potential. The diagonal term $\Delta g_i(t) S_i$ is taken to be positive in sign. It describes an excitatory feedback current representing the effect of post inhibitory rebound and does not involve synaptic processing.

A discrete time approximation of the neuronal dynamics may be obtained by first formally integrating (1) (with $V_i(0) = 0$) to obtain

$$\begin{aligned} V_i(t) \;\; = \;\; & \int_0^t \mathrm{d}t' \left[\sum_{k=1}^{N} \Delta g_{ik}(t') S_{ik}/C_i + \Delta g_i(t') S_i / C_i \right] \exp(-(t-t')/\tau_i) \\ & \times \mathrm{T} \left[\exp\left(- \int_{t'}^{t} \mathrm{d}t'' \sum_{j=1}^{N} \Delta g_{ij}(t'')/C_i \right) \right]. \end{aligned} \tag{2}$$

The symbol T denotes the time ordering operator and $\tau_i := R_i C_i$ is such that τ_i^{-1} defines the rate at which the membrane potential decays to rest in the absence of any synaptic conductance changes. A simple model of neuronal input that allows evaluation of (2) is to assume that neuron i receives an impulse of size g_{ij} each time that neuron j fires. Thus

$$\Delta g_{ij}(t + t_d) = g_{ij} \sum_{n \geq 1} \delta(t - A_j^n) \,, \tag{3}$$

where A_j^n is the time at which the j^{th} neuron fires for the n^{th} time since $t = 0$, and $\delta(x)$ denotes the Dirac-delta function. The synaptic delay time t_d is included to account for the time between the arrival of a signal at a synapse and the resulting change in resting potential of the neuron. In a similar fashion, we write the post inhibitory rebound current in the form

$$\Delta g_i(t + t_p) = g_i \sum_{n \geq 1} \delta(t - B_i^n) \,, \tag{4}$$

where B_i^n represents the time at which the i^{th} neuron rebounds for the n^{th} occasion and t_p is the delay time for post inhibitory rebound to take effect. The nth firing and rebounding times are defined by

$$A_j^n = \inf\{t \mid V_j(t) \geq h; t \geq A_j^{n-1} + t_R\}\,, \quad B_j^n = \inf\{t \mid V_j(t) \leq \kappa; t \geq B_j^{n-1}\}\,, \tag{5}$$

respectively. Here t_R is the absolute refractory period such that a neuron is incapable of firing within a time t_R after it last fired. The quantities h and κ measure the thresholds for firing and rebounding respectively. In general, the A_j^n and B_j^n lie on a lattice generated by t_d, t_p, t_R, and the first times that firing and rebounding occur.

For simplicity, we set $t_p = t_R = t_d$ and proceed by breaking the integral in (2) into $[0, t_d]$ and $[t_d, t]$. The integral over $[0, t_d]$ is treated as a boundary term which is determined by the state of the network over the interval $[-t_d, 0]$. We choose initial conditions such that the first firing and rebounding times are multiples of t_d. In this case all subsequent firing and rebounding times are multiples of t_d. For any function f, we may write

$$\sum_{n\geq 1} f(A_j^n) = \sum_{m=0}^{\infty} f(mt_d)a_j(m), \qquad \sum_{n\geq 1} f(B_j^n) = \sum_{m=0}^{\infty} f(mt_d)b_j(m), \tag{6}$$

where $a_j(m)$ and $b_j(m)$ are the *firing* and *rebounding* functions defined by

$$a_j(m) = \begin{cases} 1 & A_j^n = mt_d \\ 0 & \text{otherwise} \end{cases}\,, \qquad b_j(m) = \begin{cases} 1 & B_j^n = mt_d \\ 0 & \text{otherwise} \end{cases}\,. \tag{7}$$

Hence we deduce that

$$\begin{aligned} V_i(m) \;=\; & \sum_k \sum_{r=1}^{m} w_{ik} a_k(m-r)\gamma_i^{r-1} \exp(-\sum_j \sum_{s=1}^{r} \tilde{w}_{ij} a_j(m-s)) + \\ & \sum_{r=1}^{m} w_i b_i(m-r)\gamma_i^{r-1} \exp(-\sum_j \sum_{s=1}^{r} \tilde{w}_{ij} a_j(m-s)) \end{aligned} \tag{8}$$

for $t = mt_d$. (In (8), we have set t_d to unity for clarity and introduced $\gamma_i = \mathrm{e}^{-1/\tau_i}$, $w_{ij} = g_{ij}S_{ij}/C_i$, $\tilde{w}_{ij} = g_{ij}/C_i \geq 0$ and $w_i = g_i S_i/C_i > 0$.) At non-integer multiples of the fundamental time delay t_d, the neuronal dynamics are given by

$$V_i(t) = \mathrm{e}^{-(t-m)/\tau_i} V_i(m), \qquad m = 0, 1, 2, \ldots \qquad m < t < (m+1). \tag{9}$$

We re-write (8) as a first-order iterative equation for $V_i(m)$

$$V_i(m) = \left[\gamma_i V_i(m-1) + \sum_k w_{ik} a_k(m-1) + w_i b_i(m-1)\right] \times \exp\left\{-\sum_j \tilde{w}_{ij} a_j(m-1)\right\} \tag{10}$$

with the firing and rebounding functions taking the form $a_i(m) = \Theta(V_i(m) - h)$, $b_i(m) = \Theta(\kappa - V_i(m))$; Θ being the step function

$$\Theta(x) = \begin{cases} 1 & \text{if } x \geq 0 \\ 0 & \text{if } x < 0 \end{cases}\,. \tag{11}$$

To illustrate the dynamical equations (9) and (10), we show the output from one neuron in a network of six in figure 1. From the top, the three lines depict the threshold for firing, the resting potential of the neuron and the threshold for rebounding. The figure demonstrates that a neuron with post inhibitory rebound within a neuronal population may undergo regular self-sustained oscillations. For example, a neuron may receive an inhibitory input which drives it below the threshold for rebounding. After a delay (in this instance of one time unit), the membrane potential can increase above the firing threshold due to the injection of the post inhibitory rebound current. If the neuron continues to receive regular inhibitory input from the rest of the population, it will continue to fire in the same pattern.

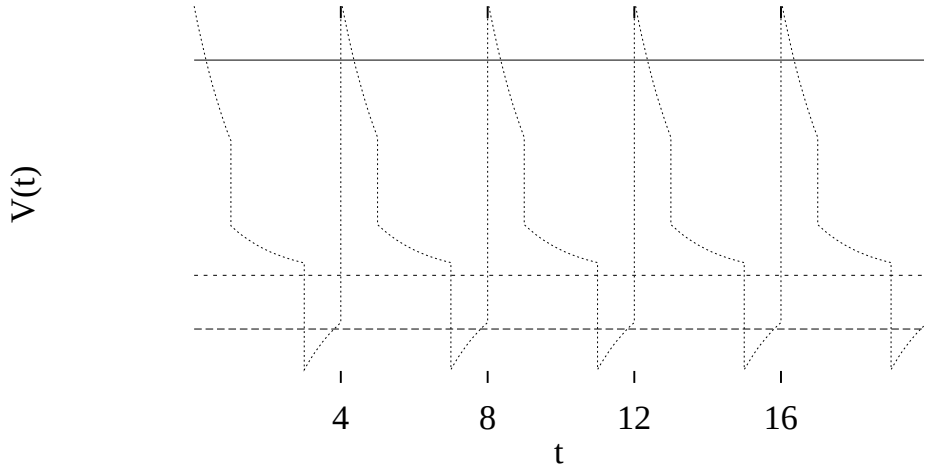

Figure 1: Illustrative membrane dynamics for a member of neuronal population with post inhibitory rebound. Discrete units of time are integer multiples of t_d.

Before analysing the complex dynamics of PIR networks further, we consider the case of a single neuron with external input I satisfying

$$V(m+1) = [\gamma V(m) + w_a a(m) + w_b b(m) + I]\, \mathrm{e}^{-\tilde{w} a(m)} \tag{12}$$

with $\gamma < 1$, $\tilde{w} \geq 0$. This can be thought of as studying how one such neuron can behave within a large population. One of the features of the single neuron dynamics is the possibility of (bands of) chaos as we vary the input. To observe when this occurs, we examine the Liapunov exponent of (12) defined by

$$\begin{aligned} \lambda(V) &= \lim_{n\to\infty} \frac{1}{n} \sum_{m=0}^{n-1} \log \frac{\mathrm{d}V(m+1)}{\mathrm{d}V(m)} = \log\gamma - \tilde{w} \lim_{n\to\infty} \frac{1}{n} \sum_{m=0}^{n-1} \Theta(V(m+1) - h) \\ &= \log\gamma - \tilde{w}\rho(V)\,, \end{aligned} \tag{13}$$

where we have introduced the average firing rate

$$\rho(V) = \lim_{n\to\infty} \frac{1}{n} \sum_{m=1}^{n} a(m)\,. \tag{14}$$

For the neuron, this is a natural quantity characterizing response, but may also be taken as a rotation number for the map dynamics of (12) (Tresser 1983). If the limit (14) does not exist, we use the lim inf and lim sup to define rotation intervals, and hence a Liapunov interval – see Section 3. For $\tilde{w} > 0$, the limit in (14) exists and is independent of initial conditions. Hence, $\lambda(V) < 0$, independently of V and the resultant dynamics of the map (12) are not chaotic. However, hysteresis is possible, as will be shown in Section 3. Now suppose $\mathrm{e}^{-\tilde{w}}\gamma > 1$, that is, we extend the allowed range of $\tilde{w}$ to $\mathbf{R}$. In this case, the dynamics can become chaotic. However, this scenario is biologically implausible since it implies a decrease in synaptic conductance at the synapse. It follows that to have chaotic solutions when $N > 1$ requires $\exp(-\sum_j \tilde{w}_{ij})\gamma_i > 1$ for at least one i.

3 A piecewise linear discontinuous circle map

3.1 Defining the map

Neuronal population dynamics of the type described by equation (1) without post inhibitory rebound have previously been investigated by Bressloff & Stark (1990). They demonstrated the insight that could be gained into the dynamical system corresponding to (12) from the reduction to a piecewise linear circle map – in their case, with a single discontinuity. A piecewise linear circle map formulation is attractive from a mathematical standpoint since it is a nonlinear dynamical system which is amenable to detailed analysis (Campbell, Galeeva, Tresser & Uherka 1995, López 1995). In the biological domain, circle maps have been useful in modelling mode-locking (Bauer & Martienssen 1991), cardiac arrythmias (Bub & Glass 1995, Glass 1991, Glendinning 1995) and neural networks (Aihara et al. 1990, Bressloff & Stark 1990, Zeller, Bauer & Martienssen 1995). In addition, they have been applied to, for example, models of Josephson junctions (Jensen, Bohr, Christiansen & Bak 1983), electrical conductivity in barium sodium niobate (Martin & Martienssen 1986), lasing (Marriott & Delisle 1989) and chemical reactions (Lauterborn & Eick 1988).

We define $x_m := V(m) - h$ and introduce the parameters $\delta = h - \kappa$, $\mu = \gamma \mathrm{e}^{-\tilde{w}}$, $\nu = \gamma$ and $A = I - h(1-\gamma)$. The dynamics of a single PIR neuron is then governed by the map

$$x_{m+1} = \mathcal{F}(x_m) = \begin{cases} \mu x_m + A - B & x_m \geq 0 \\ \nu x_m + A & -\delta \geq x_m < 0 \\ \nu x_m + A + w_b & x_m < -\delta \end{cases} , \tag{15}$$

where $B := (A+h)(1-\mathrm{e}^{-\tilde{w}}) - w_a \mathrm{e}^{-\tilde{w}}$ (see figure 2). $\mathcal{F}$ as a map depends on six parameters: A, B, μ, ν, δ and w_b. A is interpreted as the global input from the surrounding neuronal population and will be used as a bifurcation parameter. We concentrate on the case $B > A > 0$ and hence $C := A - B < 0$, since otherwise trivial fixed point dynamics result. In this situation bounded dynamics is confined to an invariant interval Σ. In addition, we have $\mu > 0$, $0 < \nu < 1$, $w_b > 0$ and $\delta > 0$. Note that the biological restriction, $0 < \mu < 1$, discussed at the end of Section 2, has been relaxed. Unlike the original model of Bressloff & Stark (1990), a single neuron with post inhibitory rebound has two discontinuities instead of one. As we show, this can lead to a richer dynamics for our basic neuron including: transitions to and from chaos as A varies; loss of monotonicity and jumps in the firing rate for quasiperiodic behaviour; and hysteretic transitions

between periodic orbits. We also outline how a more exhaustive analysis of the periodic and chaotic dynamics could be obtained, as has been achieved for related maps in (Campbell et al. 1995, Glendinning 1995, López 1995). We do not enter into great detail. Our interest is to note the possible types of asymptotic behaviour, rather than catalogue *all* possible periodic orbits and derive *all* transition conditions. Note that we have referred to just two discontinuities. The one at zero is, in a sense, removed when the interval map defined by (15) is considered as a (lift of) a degree one circle map (so that the theory of Keener (1980) and Tresser (1983) can be applied). To ensure the resultant map is of degree one, the invariant interval must be scaled to unity. We proceed assuming this is done and set $B = 1$. However, that is not to say that the discontinuity at zero is unimportant. In fact, whilst the discontinuity at the end of the invariant interval can point to chaos for the bilinear map, it is largely the interaction of the map dynamics with the discontinuities at zero and $-\delta$ that shape the bifurcation diagram for the trilinear map.

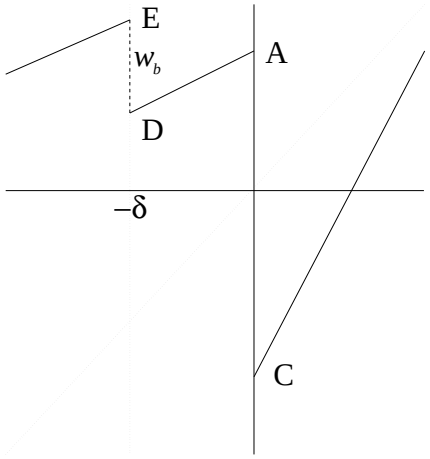

Figure 2: The piecewise linear map model $\mathcal{F}$ of the PIR neuron.

3.2 The Liapunov interval

To distinguish between (quasi-)periodic and chaotic behaviour, we derive a formula for the Liapunov exponent. The calculation is straightforward as the map is piecewise linear.

$$\lambda(x) = \lim_{n\to\infty} \frac{1}{n} \log \prod_{m=0}^{n-1} \frac{\mathrm{d}x_{m+1}}{\mathrm{d}x_m} = \lim_{n\to\infty} \frac{1}{n} \log(\nu^{(1-\rho)n}\mu^{\rho n}) = \log\nu + \rho(x)\log\left(\frac{\mu}{\nu}\right), \qquad (16)$$

where we have used that fact that the map comprises of two pieces of equal slope ν on the left handside. This is a usable form of (13) since μ and ν are given whilst $\tilde{w}$ is only implicitly defined through the bifurcation parameter A. Equation (16) also shows that $\mu > 1$ is a necessary condition for chaotic dynamics. When the limit $\rho(x)$ does not exist, the average firing rate or rotation number is defined as the set of limit points of the sequence $\sum_{m=1}^{n} a(m)/n$. The union

of such sets over the invariant interval Σ is given by $[\underline{\rho}, \overline{\rho}]$ where

$$\underline{\rho}(x) = \inf_{V\in\Sigma} \liminf_{n\to\infty} \sum_{m=1}^{n} \frac{a(m)}{n}, \qquad \overline{\rho}(x) = \sup_{V\in\Sigma} \limsup_{n\to\infty} \sum_{m=1}^{n} \frac{a(m)}{n} \tag{17}$$

It follows that the Liapunov exponent is replaced by a Liapunov interval $[\underline{\lambda}, \overline{\lambda}]$ defined in the obvious way. A non-trivial rotation interval is an indicator of complex dynamics, and positive topological entropy for piecewise linear maps (Tresser 1983, Gora & Boyarsky 1991). However, it seems better to base an observation of deterministic chaos upon $\lambda(x) > 0$. As an example, Bub & Glass (1995) note that their piecewise linear map exhibits 'banded chaos' when $\lambda > 0$ and the rotation interval collapses to a point.

3.3 Invariant intervals and conditions for chaos

Before equation (15) can be regarded as having 'circle map dynamics', we must consider when an appropriate invariant interval exists, and what are suitable ranges for the variation of the bifurcation parameter A. The map has a fixed point at $\bar{x} = (1-A)/(\mu-1)$. This is stable/unstable as μ is less than or greater than one. Whichever is the case, nontrivial dynamics can only occur while this point remains outside the invariant interval Σ as A varies. Moreover, when $C > -\delta$ (that is, $A > 1-\delta$), then $\mathcal{F}$ reduces to a bilinear map and has just one discontinuity (at the endpoints). Hence, in addition to the Liapunov criterion for chaos, we may use a geometric condition (Keener 1980, Tresser 1983). Namely, when the ends of the two-piece map overlap nontrivially,

$$A > \frac{1-\nu}{\mu-\nu}, \tag{18}$$

then chaotic dynamics ensue. We introduce two quantities

$$E := \mathcal{F}([-\delta]_-) = -\nu\delta + A + w_b, \qquad D := \mathcal{F}([-\delta]_+) = -\nu\delta + A, \tag{19}$$

namely, the heights of $\mathcal{F}$ on either side of the discontinuity at $-\delta$. By considering figure 2, we see that *a priori* there are four possibilities for Σ, as determined by the relative heights of A & E and C & D, respectively. In fact, it is straightforward to show that D cannot be a lefthand endpoint: Σ is either $[C, A]$ or $[C, E]$. We distinguish three cases of map geometry: the first two allow for new dynamics compared to Bressloff & Stark (1990).

Case (i). If $A > E$ and $C < D$, then Σ is $[C, A] = [A-1, A]$ and $w_b < \nu\delta < 1$. Hence, nontrivial dynamics occur for $A < \min(1, 1/\mu)$. On the left of a bifurcation diagram in A, the map will be trilinear. Once A increases beyond $1-\delta$, the map is bilinear and any transition to chaos in this region can be predicted using the overlap rule (18).

Case (ii). Suppose $E > A$ and $C < D$, so that $\min(1, w_b) > \nu\delta$. For small A, Σ is $[C, E]$ but as A increases, there are two possibilities. If E hits $\bar{x}$ when $A = A_E$, say, and $A_E < 1-\delta$, then the dynamics collapse when $A = A_E$ and there are no nontrivial bilinear dynamics. Alternatively, if $A_E > 1-\delta$, then at $A = 1-\delta$, the map becomes bilinear and the invariant interval jumps discontinuously to $[C, A]$.

Case (iii). When $D < C$, that is $\nu\delta > 1$, the discontinuity at $-\delta$ is not included in the invariant interval. The map is bilinear for all relevant variation of the bifurcation parameter A, and nothing more than Bressloff & Stark dynamics can be observed. Biologically, the values of the model parameters automatically mean that PIR does not affect the neuron.

The Keener overlap criterion (18) provides a simple characterization of when chaos occurs. This is not possible in general. However, the use of (renormalized) induced maps allows the application of the rule to boxes centred on $-\delta$ or zero which are invariant under higher iterates of the map $\mathcal{F}$. In this way, a series of Keener rules can be derived. We give an example of this procedure within the following notation. Simple periodic orbits of the map can be explicitly described. For example, a $(p,\ q,\ r)$-orbit on $[C, A]$ is a periodic orbit of period $p+q+r$ which visits the three parts of the domain $[C, -\delta)$, $[-\delta, 0)$ and $[0, A)$, p, q and r times respectively, and is stable if $\nu^{p+q}\mu^r < 1$. Simple primary orbits of the form $(0, 1, n)$ or $(1, 0, n)$ are stable for $\nu\mu^n < 1$. It is straightforward to calculate that the leftmost points of such orbits are given by

$$x^{(1)} = \frac{\left(\sum_{m=1}^{n}\mu^m\right)A - \left(\sum_{m=1}^{n-1}\mu^m\right)}{1-\mu^n\nu}, \quad x^{(2)} = \frac{\left(\sum_{m=1}^{n}\mu^m\right)A - \left(\sum_{m=1}^{n-1}\mu^m\right) + \mu^n w_b}{1-\mu^n\nu}, \quad (20)$$

respectively. Many of the features of the bifurcation diagrams can be understood in terms of periodic orbits like these, and more importantly when they cease to exist: for example, when a point on the orbit coincides with one of the discontinuities as we vary A. Since μ and ν are *not* varied as parameters, the interaction with the discontinuities determines much of the bifurcation dynamics. It is the presence of the middle piece of map acting on $(-\delta, 0)$ that introduces the 'copies' of the Bressloff & Stark dynamics (see figure 10). In addition, after colliding with a discontinuity (O or $-\delta$), a primary periodic orbit typically undergoes a 'Farey tree'-type bifurcation (Ringland, Issa & Schell 1990) which thus generates period k solutions, where k is limited mathematically by the resolution of the bifurcation diagram, and biologically by minimum feasible currents (see figures 5 and 11). Of course, this is also to be found in (Bressloff & Stark 1990), for example. The novelty with two discontinuities is that the discontinuity at $-\delta$ can also trigger such behaviour as A varies, and the two discontinuities compete with each other to create new features, for instance, hysteresis.

We now outline how the overlap criterion can be applied to an induced map. For example, consider a symmetric ϵ–neighbourhood about $-\delta$ and the map $\mathcal{G}$ induced by the action of $\mathcal{F}^3$ on $(-\delta-\epsilon, -\delta)$ and $\mathcal{F}^2$ on $(-\delta, -\delta+\epsilon)$. In order that $\mathcal{G}$ maps into $(-\delta-\epsilon, -\delta+\epsilon)$, we require $\mu\nu,\ \mu^2\nu < 2$. We suppose that $\mu > 1$ so that chaos is possible. The map $\mathcal{G}$ can be written

$$\mathcal{G}(z) = \begin{cases} \mu^2\nu z - \mu^2\nu\delta + \mathcal{F}^3([-\delta]-) & z \in (-\epsilon, 0) \\ \mu\nu z - \mu\nu\delta + \mathcal{F}^2([-\delta]+) & z \in (0, \epsilon) \end{cases}, \quad (21)$$

and is well defined for $\mu E > 1 - \nu\delta$. It is straightforward to derive conditions on A so that the induced map remains in the ϵ–neighbourhood of zero. Assuming these are satisfied, there is overlap for the induced map and hence chaos if, in addition,

$$A < \frac{\nu}{\mu}((\mu-1)\delta + (\mu+1)\epsilon) + \frac{1}{\mu} - w_b\,. \quad (22)$$

Similar conditions can be easily generated for other invariant boxes and induced maps. However, these generalized Keener rules seem impractical. A parameter space analysis for a multipart interval map arising from a relaxation oscillator (Christiansen, He, Habip, Bauer, Krueger & Martienssen 1992, He, Wang, Bauer, Habip, Krueger, Martienssen & Christiansen 1994, Guan, Wang, Da-Kai & He 1995) has similar problems with escalating complexity and cannot yield a succinct picture of the possible behaviours. A more global analysis is required to classify the transitions for the fully trilinear map in a clearer and more helpful fashion. However, such an analysis is a major digression and we do not pursue it further here. Instead, we illustrate the rich dynamical behaviour that can be generated by the trilinear map, and thereby show some of the features one would see emerge from a more general analysis.

3.4 Numerical results

We begin this more numerical subsection by illustrating the application of the overlap rules. For comparison purposes, it is important to first reproduce the bifurcation diagrams for the bilinear Bressloff & Stark map. We could do this by setting $w_b = \delta = 0$. Instead, we show how pure bilinear behaviour can occur for nonzero values (Case(iii)) because of the size of the invariant interval: exactly the same bifurcation diagrams are then obtained – see figures 3 and 4. Figure 3(a) is the bifurcation diagram illustrating the complex structure of the periodic orbits whilst figure 3(b) shows how the Liapunov exponent follows the pattern of a self-similar devil's staircase. (Bressloff & Stark did not consider the Liapunov exponent, but equation (13) is discussed in Bressloff (1991).) In figure 3(a), the regular arrangement of orbits is according to a Farey sequence, with mediants, in two directions (cf. Ringland et al. (1990) with $s \to \infty$). The order of mediant orbits can be found by concatenation of the enclosing lower order orbits. Plateaus corresponding to primary orbits (as indicated by the firing map/rotation number) are interrupted when a periodic orbit hits the origin as A varies. This causes a 'Farey tree' bifurcation to a 'very high order' periodic orbit, one whose order is limited mathematically only by the resolution of the diagram. Ringland et al. (1990) have a two part piecewise linear map embedded as a limit of their two parameter family of double extremum maps. They investigate the variation of quasiperiodic behaviour and show how the 'Farey tree' bifurcation might be viewed as the 'ghost' of a degenerate coincidence of lines of period-doubling, saddle-nodes and superstability. In this example, the Liapunov exponent decreases because $\mu < \nu$. Note, too, the reduction to fixed point dynamics once $A = 1$. In figure 4, we see how the periodic behaviour becomes chaotic: the Liapunov exponent graph confirms the theory (18) which predicts transition to chaos when $A = 2/3$.

In figure 5, we show an example of Case (ii) dynamics, along with the associated Liapunov exponent (which indicates the onset of chaos at approximately 0.65). With $\delta = 0.1$, the whole figure is dominated by trilinear dynamics and even the quasiperiodic regime loses the symmetry typical of the bilinear map. Bilinearity only appears at $A = 1 - \delta = 0.9$, by which time the overlap rule (18) ensures chaos. In figure 6, we show the average firing and rebounding rates for this parameter set. For both the Liapunov exponent and the firing rate, the effect of PIR is clear: jumps and lack of monotonicity in the devil's staircase. For the Liapunov exponent, one can see that the jumps are associated with a periodic orbit hitting the discontinuity at $-\delta$ as A is varied. Typically the same period orbit cannot be sustained on the smaller piece of the map. And if the period changes, then so will the firing rate and hence the Liapunov exponent. This

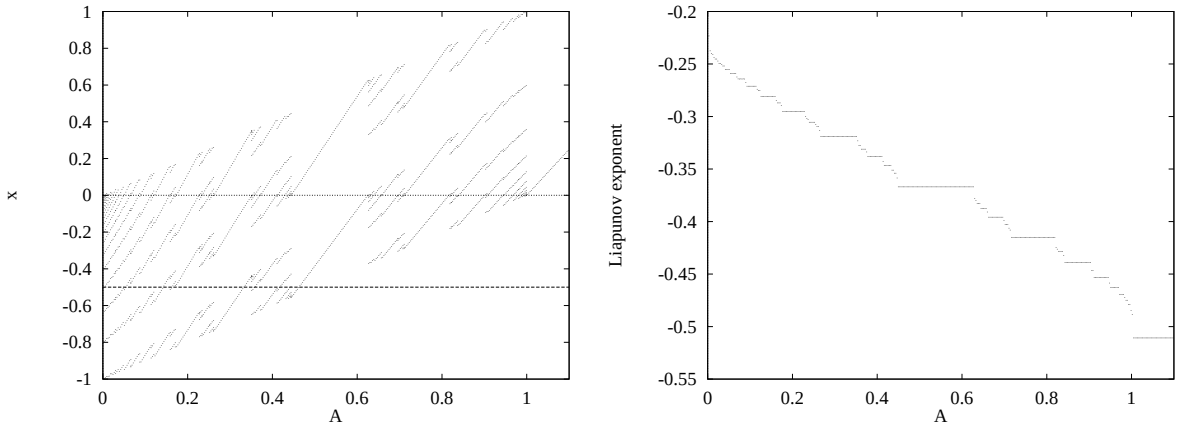

Figure 3: (a) Bifurcation diagram and (b) Liapunov exponent: Bilinear dynamics – $\mu = 0.6$, $\nu = 0.8$, $\delta = 2$, $w_b = 1.8$, $B = 1$.

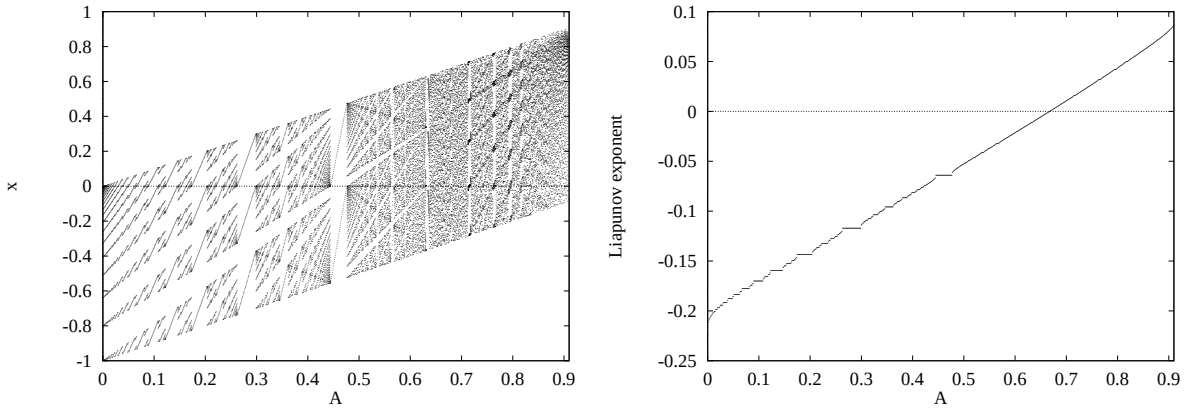

Figure 4: (a) Bifurcation diagram and (b) Liapunov exponent: Bilinear dynamics – $\mu = 1.1$, $\nu = 0.8$, $\delta = 2$, $w_b = 1.8$, $B = 1$.

jump in period at $-\delta$ can also give rise to hysteresis. Other typical features are the compressed, miniature versions of Bressloff & Stark diagrams which occur at regular intervals and increase in size with A until chaos sets in. The size of these windows is decreased if one minimises the effect of PIR, that is, reduce δ and w_b. Note, too, how the greater disparity between the μ and ν values is reflected in the increasing skewness of the branches in the central primary $(1, 0, 1)$ orbit compared to the main $(0, 1, 1)$ period 2 orbit in figure 3. In figure 7, we illustrate how for $\Sigma = [C, E]$, there can be a jump to a smaller invariant interval when the map reduces to a bilinear one at $A = 1 - \delta$. This feature is also present in figure 5, but the size of the jump $w_b - \nu\delta = 0.01$ makes the change hard to observe.

The fact that the Liapunov exponent can jump because of PIR allows for bands of chaos. That is, transitions to and from chaos within the trilinear regime. To raise the jumps in the exponent sufficiently high, we increase μ – as might be expected from the form of (16). We chose parameter values from Case (i): the results are shown in figures 8 and 9. To obtain the Liapunov intervals shown in figure 9(a) for a given A, we used 1000 initial conditions. From

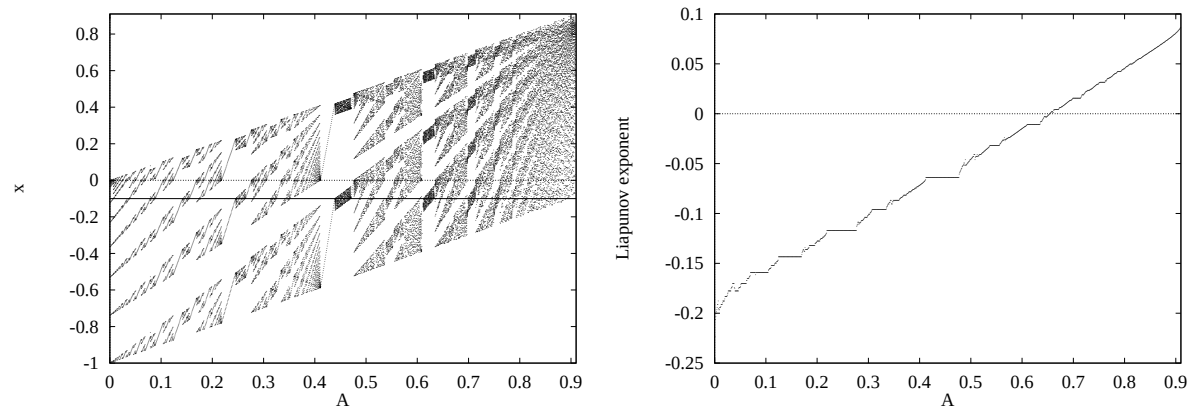

Figure 5: (a) Bifurcation diagram and (b) Liapunov exponent: Case(ii) dynamics – $\mu = 1.1$, $\nu = 0.5$, $\delta = 0.1$, $w_b = 0.06$, $B = 1$.

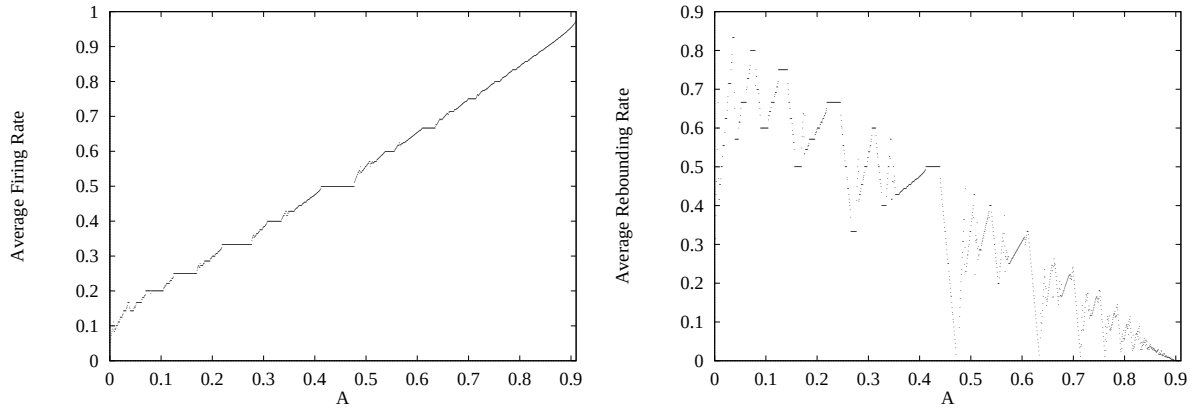

Figure 6: (a) Averaged Firing and (b) Rebounding rates: Case(ii) dynamics – $\mu = 1.1$, $\nu = 0.5$, $\delta = 0.1$, $w_b = 0.06$, $B = 1$.

each, we discarded the first 100,000 iterates as transients and then constructed the intervals from the next 10,000. If any part of $[\underline{\lambda}, \overline{\lambda}]$ crosses zero, this indicates that there are chaotic dynamics for some subset of the invariant interval.

In figure 10, we show a typical example of Case (i) map dynamics. In this instance, the transition to chaos occurs in the bilinear regime $A > 0.5$ as predicted by (18) – the increased symmetry in the second half of the figure is certainly most noticeable. In figure 11, we focus on two windows. In the first, we have a 'Farey tree' bifurcation when a periodic point hits zero, followed by a jump in periodicity when points on the high period orbits so created collide with the discontinuity at $-\delta$ near the bottom of the figure 11(a). The periodic points pass entirely above $-\delta$ when $A = 0.5$. At the top of this figure, near $A = 0.4875$ for example, we note an interesting feature again arising through the extra discontinuity at $-\delta$. Namely, a jump to a different periodic orbit. This is a sign that hysteresis can occur. It is this feature that we show clearly in figure 11(b) for a much lower order periodic orbit. We have plotted the map dynamics for both increasing and decreasing A to illustrate the hysteresis and how it is associated with

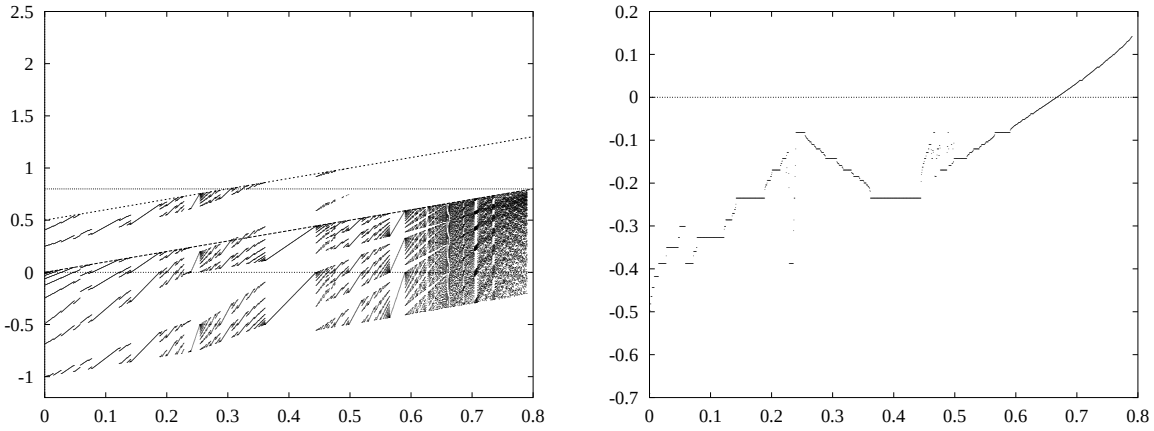

Figure 7: (a) Bifurcation Diagram and (b) Liapunov Exponent: Invariant Interval Jumps – $\mu = 1.25$, $\nu = 0.5$, $\delta = 0.5$, $w_b = 0.75$, $B = 1$.

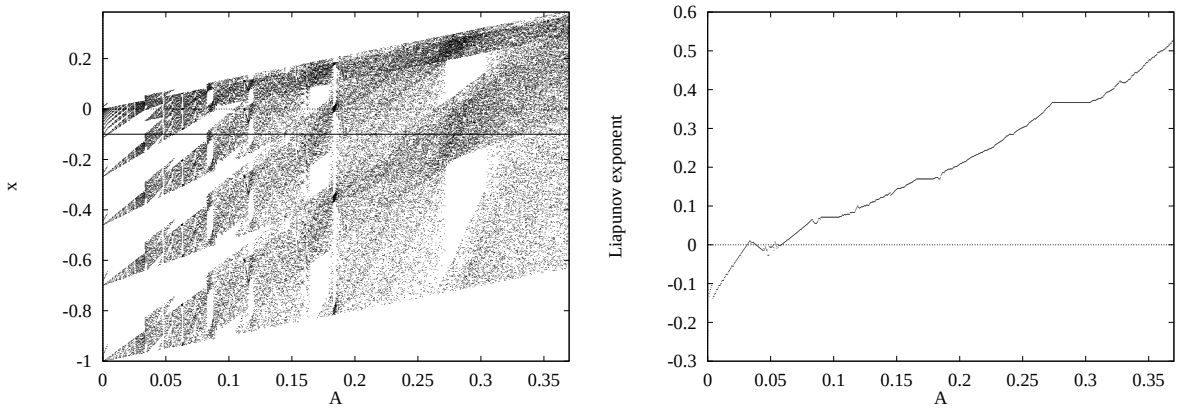

Figure 8: (a) Bifurcation diagram and (b) Liapunov exponent: Bands of chaos – $\mu = 2.6$, $\nu = 0.8$, $\delta = 0.1$, $w_b = 0.1$, $B = 1$.

coexistence of periodic orbits and collisions with $-\delta$.

Before we return to analysing networks of PIR neurons, we show how the piecewise linear nature of the map allows explicit analysis of the hysteresis and how it can appear for these primary orbits with biologically realistic values of μ and ν. Namely, $\mu \leq \nu < 1$. Hysteresis cannot occur when $\delta = w_b = 0$. The period two $(1, 0, 1)$-orbit in figure 11(b) hits $-\delta$ when

$$A = A_2 = \frac{-\delta(1 - \mu\nu) + 1 - \mu w_b}{\mu + 1}, \tag{23}$$

and the period three $(0, 2, 1)$ orbit when

$$A = A_3 = \frac{-\delta(1 - \mu\nu^2) + 1}{\mu\nu + \mu + 1}. \tag{24}$$

For the period 3 orbit to be feasible, we require $D < 0$, $(A < \nu\delta)$ so that two successive iterates in

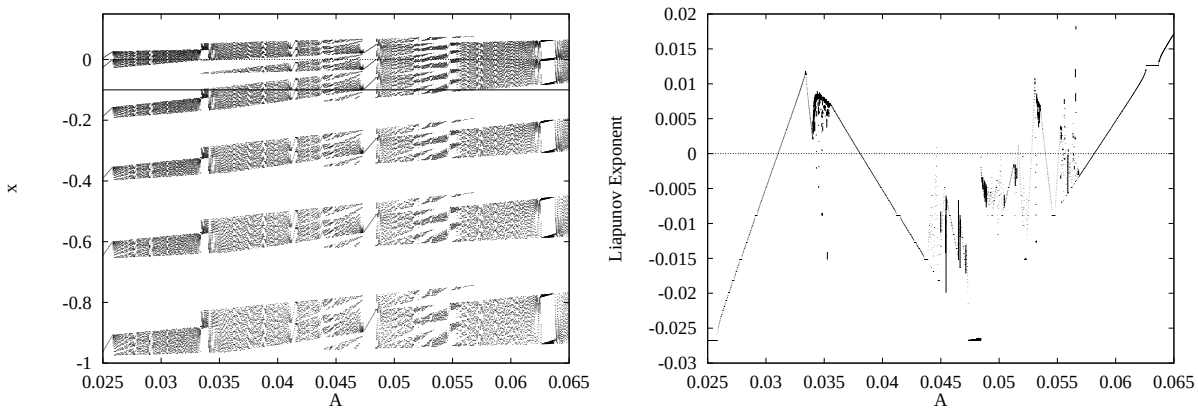

Figure 9: Bands of chaos: (a) close up and (b) Liapunov intervals $\mu = 2.6$, $\nu = 0.8$, $\delta = 0.1$, $w_b = 0.1$, $B = 1$.

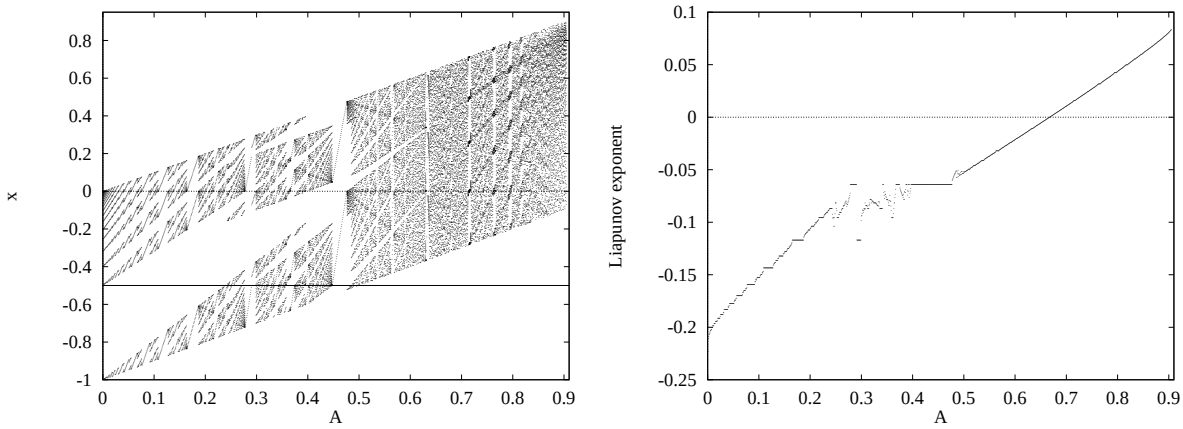

Figure 10: (a) Bifurcation diagram and (b) Liapunov exponent: Case(i) dynamics $\mu = 1.1$, $\nu = 0.8$, $\delta = 0.5$, $w_b = 0.3$, $B = 1$.

$(-\delta, 0)$ are possible. Now when $\delta = w_b = 0$, we always have $A_2 < A_3$ and no hysteresis is possible: the usual 'Farey tree' bifurcation will occur. However, once PIR is included, there is a window of μ and ν values where hysteresis can occur, nominally bounded by ν and μ values such that $A_2 = A_3$. For example, equality can occur when $\mu = 0$ and $\mu = (\nu^2\delta - \nu + w_b)/(\nu^2\delta - w_b\mu - w_b)$. These correspond to A values of $1 - \delta$ and $(\nu\delta(\nu - 1) + w_b)/\nu$ respectively. The latter value can only be attained when $w_b < \nu\delta$, a defining condition for Case (i) dynamics. However, these windows are further restricted by the loci $A = \nu\delta$ (as mentioned above) and $A = \nu/(\mu\nu + \nu + 1)$ (the value when the middle point of the period 3 orbit hits the origin). In addition, for A increasing, the period 3 orbit can be extinguished when the A value at which the period 2 orbit hits $-\delta$ overtakes that for the collision of the midpoint of the period 3 orbit with the discontinuity at zero. Repeating such an analysis for other pairs of periodic orbits is time-consuming and we do not pursue it further here.

In this section, we have established that, even at biologically realistic parameter values, the response of the PIR neuron to its global input can depend on whether the surrounding network

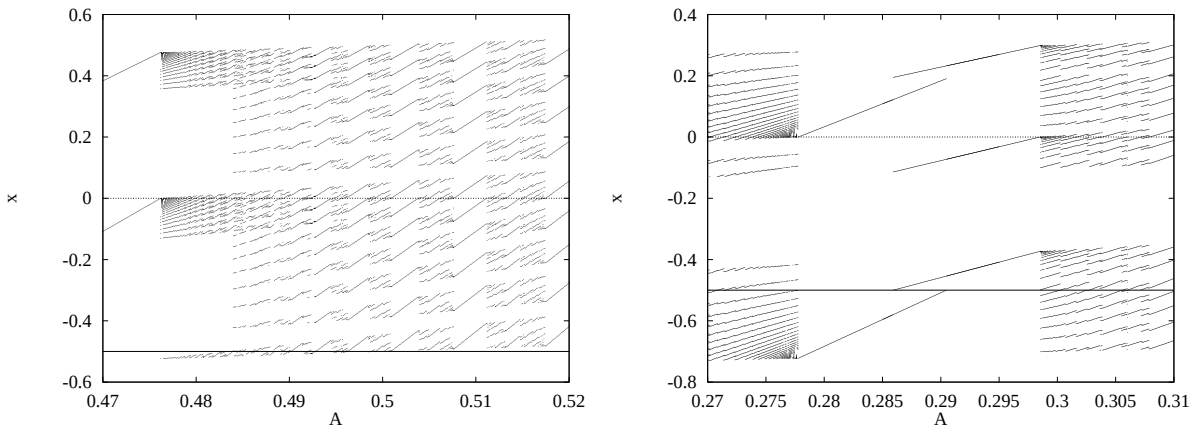

Figure 11: Two close ups: (a) double jumps and (b) hysteresis $\mu = 1.1$, $\nu = 0.8$, $\delta = 0.5$, $w_b = 0.3$, $B = 1$.

activity is increasing or subsiding. This hysteresis cannot occur in the absence of PIR. Moreover, we have identified how this phenomenon is linked to the interaction of the dynamics with the discontinuities at $-\delta$ and 0.

4 Alternating rhythms in a reciprocally inhibitory network

There remain many unresolved questions about rhythm generation in networks of non-oscillatory neurons lacking endogenous pacemaking cells. Such networks or central pattern generators are known to underlie behaviours such as heartbeat (Arbas & Calabrese 1987*a*), swimming (Arshavsky et al. 1993, Roberts, Dale & Soffe 1984) and other motor patterns (Cohen, Ermentrout, Kiemel, Kopell, Sigvardt & Williams 1992, Getting 1988). In many of these neuronal networks, reciprocal inhibitory synaptic connections are found and are thought to form the basis of network oscillation: an idea first proposed in the 'half-center' oscillator model of Brown (1914). The properties that determine the network frequency and hence the period of the oscillation are thus of obvious interest.

Post inhibitory rebound is one mechanism that can allow these architectures to oscillate (Perkel & Mulloney 1974, Roberts & Tunstall 1990, Wang & Rinzel 1992). To illustrate that the model for post inhibitory rebound presented in this paper can also lead to network oscillation in a half-center network we consider a 2 neuron network as shown in figure 12. For simplicity the neurons are considered identical. Biologically plausible values for the rebound and firing thresholds of 10mV below and 40mV above resting potential respectively are taken (Johnston & Wu 1995). For arbitrary values of the membrane decay rate, anti-phase oscillations are produced by the network dependent upon the following two conditions:

- The strength of inhibition ensures that the threshold for rebound can be reached,
- The rebound current is strong enough to drive the cell membrane potential above the threshold for firing.

Network oscillation is initiated by causing one of the neurons to fire.

After an initial stimulus that causes neuron 1 to fire, the membrane potential of cell 1 decays

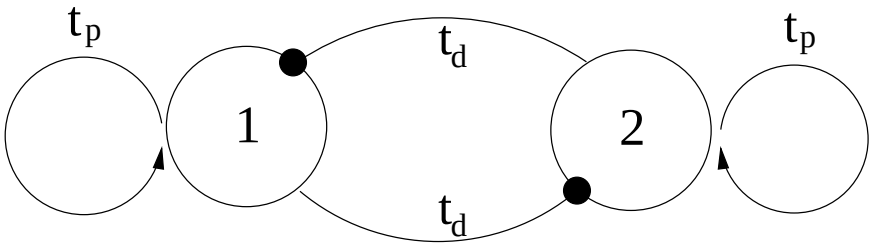

Figure 12: A two PIR neuronal network with reciprocal inhibition. Filled circles indicate inhibitory synapses. The arrowheads indicate the injection of excitatory rebound currents. t_d and t_p are respectively the time scales for conductance delays and rebound currents.

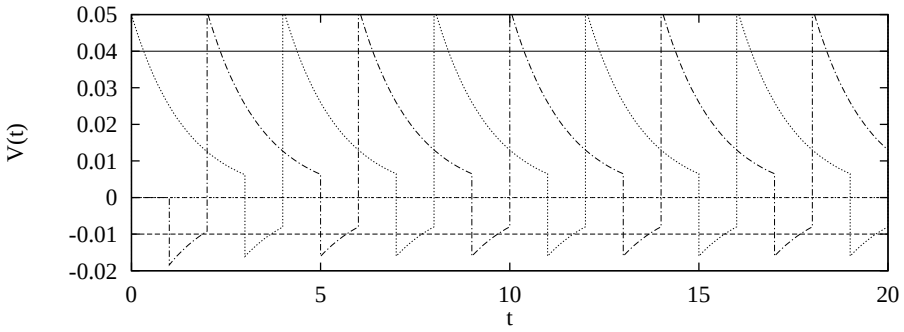

Figure 13: Membrane dynamics for two neurons with reciprocal inhibition and post inhibitory rebound.

towards the resting potential. After a synaptic conductance time delay of one unit, neuron 2 experiences an inhibitory current (due to the firing of neuron 1) that causes its membrane potential to drop below the threshold for rebound. Neuron 1 does not experience any synaptic input at this time and its membrane potential continues to decay. After a further unit delay, neuron 2 receives a positive self-feedback current that mimics the effect of post inhibitory rebound. Its membrane potential is instantaneously raised above the threshold for firing so that, one time step later, neuron 1 receives an inhibitory current that drives it below the rebound threshold. The process continues *ad infinitum* so that the rhythmic pattern is self-sustaining (see figure 13).

This example demonstrates that the model neuron is appropriate for the study of populations of neurons generating rhythms using the mechanism of post inhibitory rebound. Since many neuronal central pattern generators have very small population numbers, the two neuron scenario is not just a toy model. For example, the stomatogastric ganglion of decapod crustaceans contains about 30 neurons, most of which are motor neurons. This system produces two motor patterns, the gastric mill rhythm for chewing food and the pyloric rhythm for sorting food before it leaves the stomach. The role of hyper-polarisation-activated inward ionic currents within stomatogastric ganglion cells during rhythmic activity has been extensively investigated (Buchholtz, Golowasch, Epstein & Marder 1992, Golowasch, Buchholtz, Epstein & Marder 1992, Golowasch & Marder 1992, Turrigiano & Marder 1993). More recently a two neuron model with reciprocal inhibition and Moris-Lecar dynamics incorporating such currents has been used to model the pyloric rhythm of this system (LoFaro, Kopell, Marder & Hooper 1994).

The two neuron model introduced above, cannot reproduce voltage waveforms that resemble those measured from stomatogastric ganglion cells during rhythmic activity. That would require a more realistic choice for the synaptic conductance changes: for example, alpha functions instead of idealised spikes. However, to control muscle contractions, it is the firing and phase patterns that are of interest and how these are generated by a biologically relevant architecture of neurons. Questions about the determination of network frequency are easily considered within the proposed model. In the case considered, the network oscillation period is twice the sum of synaptic and post inhibitory rebound delays, in line with the known biology (Arshavsky et al. 1993). To obtain good quantitative agreement for firing frequencies, we merely have to include the fact that the t_p and t_d timescales are different (we discuss this in detail in Section 5).

When the restriction of external isolation is removed, the system above describes a half-center oscillator with global input. This can be used to model the effects of persistent sensory stimulation; such as occurs during the clamping of the *Xenopus* tadpole (Roberts 1990). The extension of the approach of Section 3 to the case of 2 neurons presents obvious analytical difficulties. However, populations of neurons can be readily discussed with a mean field theory (Coombes & Doole 1996). In particular, the hysteresis observed in Section 3 persists in a large network with purely inhibitory connections.

Other approaches to modelling central pattern generation in neuronal systems have included the analysis of coupled oscillators (Cohen et al. 1992, McClellan & Jang 1993, Williams 1992). In particular, this has been the case for modeling experiments on the intersegmental coordination in the lamprey spinal cord. However, this theory provides no direct link to electrophysiological data obtained at the cellular level. This is in stark contrast to the dynamical model discussed in this paper. Thresholds for firing and rebounding are easily obtained from experimental data, together with the strength of post inhibitory or hyper-polarisation-activated currents and effective delay times.

5 Discussion

In this paper we have formulated a single neuron model incorporating the effects of firing and post inhibitory rebound. From the single neuron dynamics, it is a simple matter to construct those of a population of neurons. It is this that is of interest when modelling central pattern generation in neuronal systems. For example, the spinal neuronal population in the tadpole of the frog *Xenopus* is known to generate swimming motion (Perrins & Roberts 1995*a*, Perrins & Roberts 1995*c*, Perrins & Roberts 1995*b*, Roberts & Tunstall 1990, Roberts 1990, Roberts & Tunstall 1994, Roberts, Tunstall & Wolf 1995). The intrinsic properties of the neurons that produce oscillation undoubtedly include post inhibitory rebound. Hence, simulations of large neuronal populations, incorporating post inhibitory rebound are appropriate when modeling such biological rhythms. The computational simplicity of the neuron model presented in this paper means such large scale simulations could be performed with relative ease. In contrast, more detailed (PDE) dynamical models of single neurons with active processes, such as Hodgkin-Huxley kinetics, are understandably difficult to implement at the population level (Roberts & Tunstall 1990). Systems that may be described by such studies include the thalamic reticular nucleus, the spinal cord of embryos of the tadpole *Xenopus* and the mollusc *Clione*.

For the single neuron, we reduced the dynamics to those of a piecewise linear circle map

with two discontinuities. Frequency-locking, (bands of) chaos and hysteresis can all occur. The hysteretic transition between periodic orbits can occur at biologically relevant parameter values. This suggests that a neuron can give a different response depending on whether the surrounding network activity is increasing or decreasing. This phenomenon, as well as that of *bands* of chaos, were not possible in the model without PIR of Bressloff & Stark (1990). This illustrates the richer dynamics of our basic neuron model. Full network dynamics can be treated in terms of coupled piecewise linear discontinuous circle maps and are currently under investigation.

The principle of using simple coupled elements to model neural populations at the network level is a common one within the field of artificial neural networks. Indeed, this approach has been adopted for the study of locomotor rhythm generation in the spinal cord of the lamprey (Cohen et al. 1992). However, in this instance the elements from which the population is built are simple oscillators that have no direct counterpart in the biological world. By considering a neuron description based upon leaky integrator shunting equations with hyper-polarisation-activated currents, we have maintained contact with biological realism and avoided such shortcomings.

For simplicity the effects of refractoriness have been neglected. Mechanisms underlying such phenomenon will undoubtedly include interactions between ionic currents and time and voltage dependent membrane properties. However, the description of relative refractory period first proposed by Bressloff & Taylor (1991) is one convenient way of incorporating such an effect. Throughout this paper we have also assumed, that the time delay for synaptic conductance is the same as the time delay for post inhibitory rebound to take effect. However, biology dictates that this need not be the case. In fact, the latter time delay can be as large as 10-100 times the size of the former. This is of importance since the two delay times are the main factors determining cycle period in networks with reciprocal inhibition. An extended theory, keeping the two time scales separate is developed elsewhere (Coombes, Doole & Campbell 1996) and yields oscillation periods comparable with those found in biological systems for simple neuronal architectures with reciprocal inhibition.

At this level of description, we have neglected the dendritic structure of neurons and treated them as single compartments. Furthermore, no electrical synapses have been considered. The removal of these restrictions is studied elsewhere (Coombes 1996). In many central pattern generators, definite phase relationships are established between component units and it may be that these extra structures are involved. Evidence to support this notion includes the recent discovery that diffusive coupling of nonlinear neural oscillators may lead to *dephasing* (rather than synchrony) (Han, Kurrer & Kuramato 1995, Sherman & Rinzel 1992) and the existence of bidirectional electrical synapses between pairs of motoneurones on the same side of the spinal cord in the *Xenopus* tadpole (Perrins & Roberts 1995*a*, Perrins & Roberts 1995*c*, Perrins & Roberts 1995*b*).

References

Aihara, K., Takabe, T. & Toyada, M. (1990), 'Chaotic neural networks', *Physics Letters A* **144**(6,7), 333–340.

Angstadt, J. D. & Calabrese, R. L. (1989), 'A hyperpolarisation activated current in heart interneurons of the medicinal leech', *Journal of Neuroscience* **9**(8), 2846–2857.

Arbas, E. A. & Calabrese, R. L. (1987*a*), 'Ionic conductances underlying the activity of interneurons that control heartbeat in the medicinal leech', *Journal of Neuroscience* **7**(12), 3945–3952.

Arbas, E. A. & Calabrese, R. L. (1987*b*), 'Slow oscillations of membrane potential in interneurons that control heartbeat in the medicinal leech', *Journal of Neuroscience* **7**, 3953–3960.

Arshavsky, Y. I., Orlovsky, G. N., Panchin, Y. V., Roberts, A. & Soffe, S. R. (1993), 'Neuronal control of swimming locomotion: analysis of the pteropod mollusc *clione* and embryos of the amphibian *xenopus*', *Trends in Neuroscience* **16**(6), 227–233.

Bauer, M. & Martienssen, W. (1991), 'Coupled circle maps as a tool to model synchronisation in neural networks', *Network* **2**, 345–351.

Bressloff, P. C. (1991), 'Stochastic dynamics of time-summating binary neural networks', *Physical Review A* **44**(6), 4005–4015.

Bressloff, P. C. & Stark, J. (1990), 'Neuronal dynamics based on discontinuous circle maps', *Physics Letters A* **150**(3,4), 187–195.

Bressloff, P. C. & Taylor, J. G. (1991), 'Discrete time leaky integrator network with synaptic noise', *Neural Networks* **4**, 789–801.

Brown, T. G. (1914), 'On the nature of the fundamental activity of the nervous centres; together with an analysis of the conditioning of rhythmic activity in progression, and a theory of the evolution of function in the nervous system', *Journal of Physiology (London)* **48**, 18–46.

Bub, G. & Glass, L. (1995), 'Bifurcations in a discontinuous circle map: a theory for a chaotic cardiac arrhythmia', *International Journal of Bifurcation and Chaos* **5**(2), 359–371.

Buchholtz, F., Golowasch, J., Epstein, I. R. & Marder, E. (1992), 'Mathematical model of an identified stomatogastric ganglion neuron', *Journal of Neurophysiology* **67**(2), 332–340.

Calabrese, R. L. (1995), Half-center oscillators underlying rhythmic movements, *in* M. A. Arbib, ed., 'The Handbook of Brain Theory and Neural Networks', MIT Press, pp. 444–447.

Campbell, D. K., Galeeva, R., Tresser, C. & Uherka, D. J. (1995), Piecewise linear models for the quasiperiodic transition to chaos, Technical Report RC 19982 (88466), IBM Research division.

Christiansen, B., He, D. R., Habip, S., Bauer, M., Krueger, U. & Martienssen, W. (1992), 'Phase-diagram of a modulated relaxation-oscillator with a finite resetting time', *Physical Review A* **45**(12), 8450–8456.

Cohen, A. H., Ermentrout, G. B., Kiemel, T., Kopell, N., Sigvardt, K. A. & Williams, T. L. (1992), 'Modelling of intersegmental coordination in the lamprey central pattern generator', *TINS: Trends in Neuroscience* **15**(11), 434–438.

Coombes, S. (1996), 'The effects of local electrical coupling upon neuronal population dynamics with post inhibitory rebound and reciprocal inhibition', *Preprint.*

Coombes, S. & Doole, S. H. (1996), 'The effects of synaptic and threshold noise in populations of neurons with reciprocal inhibition and rebound currents', *In preparation.*

Coombes, S., Doole, S. H. & Campbell, C. (1996), 'Central pattern generation in a model neuronal network with post inhibitory rebound and reciprocal inhibition', *Neural Network World (To appear).*

FitzHugh, R. (1961), 'Impulses and physiological states in models of nerve membrane', *Journal of Biophysics* **1**, 445–466.

Getting, P. A. (1988), Comparative analysis of invertebrate central pattern generators, *in* A. H. Cohen, S. Rossignol & S. Grillner, eds, 'Neural Control of Rhythmic Movements in Vertebrates', Wiley, chapter 4.

Glass, L. (1991), 'Cardiac arrhythmias and circle maps - a classical problem', *Chaos* **1**, 13–20.

Glendinning, P. (1995), 'Bifurcations and rotation numbers for maps of the circle associated with flows on the torus and models of cardiac arrhythmia', *Dynamics and Stability of Systems* **10**(4), 367–386.

Golomb, D., Wang, X.-J. & Rinzel, J. (1994), 'Synchronisation properties of spindle oscillations in a thalamic reticular nucleus model', *Journal of Neurophysiology* **72**(3), 1109–1126.

Golowasch, J. & Marder, E. (1992), 'Ionic currents of the lateral pyloric neuron of the stomatogastric ganglion of the crab', *Journal of Physiology* **67**(2), 318–331.

Golowasch, J., Buchholtz, F., Epstein, I. R. & Marder, E. (1992), 'Contribution of individual ionic currents to activity of a model stomatogastric ganglion neuron', *Journal of Neurophysiology* **67**(2), 341–349.

Gora, P. & Boyarsky, A. (1991), 'Computing the topological-entropy of general one-dimensional maps', *Transactions of the American Mathematical Society* **323**(1), 39–49.

Guan, S., Wang, B.-H., Da-Kai & He, D.-R. (1995), 'Dynamic interaction between discontinuity and noninvertibility: an analytical study', *Physical Review E* **52**(1 pt. A), 453–465.

Han, S. K., Kurrer, C. & Kuramato, Y. (1995), 'Dephasing and bursting in coupled neural oscillators', *Physical Review Letters* **75**(17), 3190–3193.

He, D. R., Wang, B. H., Bauer, M., Habip, S., Krueger, U., Martienssen, W. & Christiansen, B. (1994), 'Interaction between discontinuity and non-invertibility in a relaxation oscillator', *Physica D* **79**(2-4), 335–347.

Hodgkin, A. L. & Huxley, A. F. (1952), 'A quantitative description of membrane current and its application to conduction and excitation in nerve', *Journal of Physiology (London)* **117**, 500–544.

Jensen, M. H., Bohr, T., Christiansen, P. & Bak, P. (1983), 'Josephson junctions and circle maps', *Solid State Communications* **51**, 231.

Johnston, D. & Wu, S. M.-S. (1995), *Foundations of Cellular Neurophysiology*, MIT Press.

Keener, J. P. (1980), 'Chaotic behaviour in piecewise continuous difference equations', *Transactions of the American Mathematical Society* **261**(2), 589–604.

Kopell, N. & LeMasson, G. (1994), 'Rhythmogenesis, amplitude modulation, and multiplexing in a cortical architecture', *Proceedings of the National Academy of Science USA* **91**, 10586–10590.

Lauterborn, W. & Eick, I. (1988), 'Numerical investigation of a periodically driven laser with an intracavity saturable absorber', *Journal of the Optical Society of America: B* **5**(5), 1089–1096.

LoFaro, T., Kopell, N., Marder, E. & Hooper, S. L. (1994), 'Subharmonic coordination in networks of neurons with slow conductances', *Neural Computation* **6**, 69–84.

López, V. J. (1995), 'Order and chaos of piecewise linear maps', *International Journal of Bifurcation and Chaos* **5**(5), 1379–1394.

Marriott, C. & Delisle, C. (1989), 'Effects of discontinuities in the behaviour of a delay differential-equation', *Physica D* **36**(1-2), 198–206.

Martin, S. & Martienssen, W. (1986), 'Circle maps and mode locking in the driven electrical conductivity of the barium sodium niobate crystals', *Physical Review Letters* **56**, 1522.

McClellan, A. D. & Jang, W. (1993), 'Mechanosensory inputs to the central pattern generators for locomotion in the lamprey spinal cord: Resetting, entrainment, and computer modelling', *Journal of Neurophysiology* **70**(6), 2442–2454.

McCullogh, W. S. & Pitts, W. (1943), 'A logical calculus of the ideas immanent in nervous activity', *Bulletin of Mathematical Biophysics* **5**, 115–127.

Moris, C. & Lecar, H. (1981), 'Voltage oscillations in the barnacle giant muscle fibre', *Journal of Biophysics* **35**, 193–213.

Mulloney, B. & Perkel, D. H. (1988), The roles of synthetic models in the study of central pattern generators, *in* A. H. Cohen, S. Rossignol & S. Grillner, eds, 'Neural Control of Rhythmic Movements in Vertebrates', Wiley, chapter 11.

Mulloney, B., Perkel, D. H. & Budelli, R. W. (1981), 'Motor pattern production:interaction of chemical and electrical synapses', *Brain Research* **229**, 25–33.

Perkel, D. H. & Mulloney, B. (1974), 'Motor pattern production in reciprocally inhibitory neurons exhibiting post inhibitory rebound', *Science* **185**, 181–182.

Perkel, D. H., Mulloney, B. & Budelli, R. W. (1995), 'Quantitative methods for predicting neuronal behaviour', *Neuroscience* **6**(5), 823–837.

Perrins, R. & Roberts, A. (1995*a*), 'Cholinergic and electrical motoneuron-tomotoneuron synapses contribute to on-cycle excitation during swimming in *xenopus* embryos', *Journal of Neurophysiology* **73**(3), 1005–1011.

Perrins, R. & Roberts, A. (1995*b*), 'Cholinergic and electrical synapses between synergistic spinal motoneurons in the *xenopus laevis* embryo', *Journal of Physiology* **485**(1), 135–144.

Perrins, R. & Roberts, A. (1995*c*), 'Cholinergic contributions to excitation in a spinal locomotor central pattern generator in *xenopus* embryos', *Journal of Neurophysiology* **73**(3), 1013–1019.

Ringland, J., Issa, N. & Schell, M. (1990), 'From u sequence to farey sequence:a unification of one-parameter scenarios', *Physical Review A* **41**(8), 4223–4235.

Roberts, A. (1990), 'How does a nervous system produce behaviour? a case study in neurobiology', *Science Progress Oxford* **74**, 31–51.

Roberts, A. & Tunstall, M. J. (1990), 'Mutual re-excitation with post-inhibitory rebound: a simulation study on the mechanisms for locomotor rhythm in the spinal cord of *xenopus* embryos', *European Journal of Neuroscience* **2**, 11–23.

Roberts, A. & Tunstall, M. J. (1994), 'Longitudinal gradients in the spinal cord of *xenopus* embryos and their possible role in coordination of swimming', *European Journal of Morphology* **32**(2-4), 176–184.

Roberts, A., Dale, N. & Soffe, S. R. (1984), 'Sustained responses to brief stimuli: swimming in *xenopus* embryos', *Journal of Experimental Biology* **112**, 321–335.

Roberts, A., Tunstall, M. J. & Wolf, E. (1995), 'Properties of networks controlling locomotion and significance of voltage dependency of NMDA channels: Simulation study of rhythm generation sustained by positive feedback', *Journal of Neurophysiology* **73**(2), 485–495.

Satterlie, R. A. (1985), 'Reciprocal inhibition and postinhibitory rebound produce reverberation in a locomotor pattern generator', *Science* **229**, 402–404.

Sherman, A. & Rinzel, J. (1992), 'Rhythmogenic effects of weak electronic coupling in neuronal models', *Proceedings of the national Academy of Science USA* **89**, 2471–2474.

Skinner, F. K., Kopell, N. & Marder, E. (1994), 'Mechanisms for oscillation and frequency control in reciprocally inhibitory model neural networks', *Journal of Computational Neuroscience* **1**, 69–87.

Skinner, F. K., Turrigiano, G. G. & Marder, E. (1993), 'Frequency and burst duration in oscillating neurons and two cell networks', *Biological Cybernetics* **69**, 375–383.

Steriade, M., Jones, E. G. & Linas, R. R. (1990), *Thalamic oscillations and signalling*, John Wiley, New York.

Tresser, C. (1983), 'New kinds of transitions to positive topological entropy', *Comptes Rendus Academie Science Paris I* **296**, 729–732.

Turrigiano, G. G. & Marder, E. (1993), 'Modulation of identified stomatogastric ganglion neurons in primary cell culture', *Journal of Neurophysiology* **69**(3), 1993–2002.

Wang, X.-J. & Rinzel, J. (1992), 'Alternating and synchronous rhythms in reciprocally inhibitory model neurons', *Neural Computatiion* **4**, 84–97.

Williams, T. L. (1992), 'Phase coupling in simulated chains of coupled oscillators representing the lamprey spinal cord', *Neural Computation* **4**, 546–558.

Zeller, M., Bauer, M. & Martienssen, W. (1995), 'Neural dynamics modelled by one dimensional circle maps', *Chaos, Solitons and Fractals* **5**(6), 885–893.